

Instantaneous Local Control Barrier Function: An Online Learning Approach for Collision Avoidance

Cong Li, Zengjie Zhang, Ahmed Nesrin, Qingchen Liu, Fangzhou Liu, and Martin Buss

Abstract—This paper presents an integrated perception and control approach to accomplish safe autonomous navigation in unknown environments. This is achieved by numerical optimization with constraint learning for instantaneous local control barrier functions (IL-CBFs) and goal-driven control Lyapunov functions (GD-CLFs). In particular, the constraints reflecting safety and task requirements are first online learned from perceptual signals, wherein IL-CBFs are learned to characterize potential collisions, and GD-CLFs are constructed to reflect incrementally discovered subgoals. Then, the learned IL-CBFs are united with GD-CLFs in the context of a quadratic programming optimization, whose feasibility is improved by enlarging the shared control space. Numerical simulations are conducted to reveal the effectiveness of our proposed safe feedback control strategy that could drive the mobile robot to safely reach the destination incrementally in an uncertain environment.

Index Terms—Instantaneous local control barrier function, goal-driven control Lyapunov function, collision avoidance, autonomous navigation, constrained optimization.

I. INTRODUCTION

THE safe autonomous navigation of the mobile robot, i.e., safely navigating in priori unknown environments and reaching the target position, is important in applications such as search and rescue in dangerous environments [1], and food/drug delivery in the Covid-19 pandemic nowadays [2], etc. The predominant approach follows a mapping, planning and tracking control decoupled paradigm that forgo theoretical guarantees for efficient practical applications [3], [4], [5]. Each layer in this decoupled paradigm is designed assuming perfect execution of the connected layers. However, the actual performance of each layer in real-world environments often deviates from desirable expectations, which causes cascading errors in the classical map-plan-track architecture. These cascading errors and the associated influence is hard to be theoretically characterized and thus further to be addressed. For example, the tracking controller is designed assuming an available dynamical feasible and safe reference trajectory, which is might unavailable due to the infeasibility of the numerical optimization planning algorithm; Besides, the gap between the actual execution trajectory and the desired trajectory, caused by the inefficiency of the tracking controller, might result in unsafe issues even though a safe reference trajectory is provided by the planning layer. Besides, the decoupled

paradigm poses high requirements of hardware for efficient execution of each module, which is unavailable for low-cost platforms. Thus, this paper aims to develop an integrated perception and control approach that eliminates the cascading errors resulting from different components of the map-plan-track architecture, enjoys theoretical guarantees of safety and convergence to goal positions, and is suitable to platforms with low-end sensors and limited on-board computational resources.

A. Related works

To navigate safely in uncertain environments, the mobile robot needs to discover and react to potential collisions. Recently, control barrier functions (CBFs) emerge as an promising tool to realize collision avoidance at a control level (see [6], [7], and the references therein). Comparing with works achieving collision free at a planning level using collision cone [8], artificial potential method [9], navigation function [10], sampling based method [11], or reachable set [12], wherein a nontrivial collision check process based on a perfect map is required, CBF based solutions to avoid obstacles enjoys theoretical collision avoidance guarantees and computational efficiency [6]. Normally, CBFs are constructed using the obstacle information such as location, shape, and number [13], [14]. However, a complete knowledge of obstacles in an unstructured environment is not always available. Thus, to apply the CBF based collision avoidance strategy in uncertain environments, the online learning of obstacle related CBFs is required. The neural network (NN) parameterized CBFs are learned using a cost function that characterizes essential properties of CBFs [15], [16], [17]. The offline learning of barrier functions using expert demonstrations is adopted in [18], [19]. Besides, the CBF learning is formulated as a classification problem in [20], wherein a complete obstacle boundary is identified via the support vector machine (SVM) method. The CBF learning problem is solved through a global perspective in the works mentioned above [15], [16], [17], [18], [19], [20]. Alternatively, this work attempts to learn CBFs from a local perspective in favour of the robustness to previously-unobserved environments. The reach task to a predetermined goal position is able to be realized by a control Lyapunov function (CLF) based analytical or numerical control strategy [21], [22], which enjoys a theoretical convergence guarantee to target positions. However, either predetermined [21], [22] or learned [23], [24] CLF based control strategy is inefficient to complete long-horizon tasks in practice. We solve this problem through a divide-and-conquer approach by discovering subgoals incrementally using sensory data and further constructing GD-CLFs for the divided subtasks.

C.Li, Z.Zhang, A.Nesrin, F.Liu, and M.Buss are with the Chair of Automatic Control Engineering, Technical University of Munich, Theresienstr. 90, 80333, Munich, Germany (e-mail: {cong.li,zengjie.zhang,n.ahmed,fangzhou.liu,mb}@tum.de). Q.Liu is with the Chair of Information-Oriented Control, Technical University of Munich, 80869 Munich, Germany (e-mail: qingchen.liu@tum.de).

CBFs are often used with CLFs under a quadratic programming (QP) optimization to safely guide the mobile robot towards the desired position [25], [26], [27]. However, the resulting QP is susceptible to infeasibility (especially considering control limits), which remains as an open problem. This gap has marginally considered in existing works. A promising work [28] improves the QP feasibility by using the penalty and parameterization methods. Besides, control-sharing CBFs [29] and control-sharing CLFs [30], [31] are investigated separately to improve QP feasibility within consideration of multiple CBF or CLF constraints. However, the theoretically promising conclusions in [29], [30], [31] does not hold when CBFs and CLFs are considered together. This work attempts to improve the feasibility of the QP problem by enlarging the shared control space of multiple constraints.

B. Contributions

Comparing with related works, the contributions of our work are summarized as follows.

- A mapless safe autonomous navigation approach that rooted in perception and control is developed to enable a mobile robot to safely navigate in unknown environments and accomplish given tasks. The designed safe feedback control strategy enjoys computation efficiency and theoretical guarantees of safety, optimality, and convergence to goal positions.
- The instantaneous local control barrier functions (IL-CBFs) and goal-driven control Lyapunov functions (GD-CLFs) constraints are learned from sensory data to encode safety and task requirements, respectively. The online learned constraints empower the safe feedback control strategy with robustness to the long-horizon task in uncertain environments.
- An optimization over the volume of the shared control space among IL-CBFs, GD-CLFs, and input constraints is developed to improve the QP feasibility.

C. Paper organization

In this paper, Section II presents the preliminaries and the problem formulation. Then, the IL-CBFs and GD-CLFs learning processes are clarified in Section III and Section IV, respectively. Thereafter, the learned IL-CBFs and GD-CLFs are united through QP in Section V. Moreover, the strategy to improve the QP feasibility is shown in Section VI. The safe feedback control strategy is numerically validated in Section VII. Finally, the conclusion is shown in Section VIII.

Notations: Throughout this paper, \mathbb{R} , \mathbb{R}^+ , and \mathbb{R}_0^+ denotes the set of real, positive, and non-negative real numbers, respectively; \mathbb{N}^+ denotes the set of non-negative integers; \mathbb{R}^n is the Euclidean space of n -dimensional real vector; $\mathbb{R}^{n \times m}$ is the Euclidean space of $n \times m$ real matrices; The i -th entry of a vector $x = [x_1, \dots, x_n]^\top \in \mathbb{R}^n$ is denoted by x_i , and $\|x\| = \sqrt{\sum_{i=1}^n |x_i|^2}$ is the Euclidean norm of the vector x ; The ij -th entry of a matrix $D \in \mathbb{R}^{n \times m}$ is denoted by d_{ij} , and $\|D\| = \sqrt{\sum_{i=1}^n \sum_{j=1}^m |d_{ij}|^2}$ is the Frobenius norm of the matrix D . For notational brevity, time-dependence is suppressed without causing ambiguity.

II. PRELIMINARY AND PROBLEM FORMULATION

Before proceeding to the problem formulation, we first present the the definitions of High-order CBF (HO-CBF) and CLF focusing on the control-affine system

$$\dot{x} = f(x) + g(x)u(x), \quad (1)$$

where $x \in X \subseteq \mathbb{R}^n$ and $u(x) \in U \subseteq \mathbb{R}^m$ are system states and inputs. $f(x) : X \rightarrow \mathbb{R}^n$, $g(x) : X \rightarrow \mathbb{R}^{n \times m}$ are the drift and input dynamics, respectively.

Definition 1 (HO-CBF). [29, Definition 1] *Given the control system (1), a C^r function $h(t, x) : \mathbb{R} \times X \rightarrow \mathbb{R}$ with a relative degree r is called a (zeroing) control barrier function (of order r) if there exists a column vector $\alpha = [\alpha_1, \dots, \alpha_r]^\top \in \mathbb{R}^r$ such that for $\forall x \in \mathbb{R}^n$, $t \geq 0$,*

$$\sup_{u \in U} \left[L_g \bar{L}_f^{r-1} h(t, x) u + \bar{L}_f^r h(t, x) + \alpha^\top \xi(t, x) \right] \geq 0, \quad (2)$$

where $\bar{L}_f^r h := \left(\frac{\partial}{\partial t} + L_f \right)^r h$ is the modified Lie derivative of $h(t, x)$ along f and $r \in \mathbb{N}^+$, and the roots of the polynomial

$$p^r(\lambda) = \lambda^r + \alpha_1 \lambda^{r-1} + \dots + \alpha_{r-1} \lambda + \alpha_r, \quad (3)$$

are all negative.

Definition 2 (CLF). [32, Definition 1] *For the control system (1), a continuously differential function $V(x) : X \rightarrow \mathbb{R}$ is an exponentially stabilizing control Lyapunov function (CLF) if there exists $c_1, c_2, c_3 \in \mathbb{R}^+$ such that*

$$c_1 \|x\|^2 \leq V(x) \leq c_2 \|x\|^2 \quad (4a)$$

$$\inf_{u \in \mathbb{R}^m} [L_f V(x) + L_g V(x)u + c_3 V(x)] \leq 0. \quad (4b)$$

hold for $\forall x \in X$.

This paper we focus on a mobile robot modeled as:

$$\underbrace{\begin{bmatrix} \dot{p} \\ \dot{v} \end{bmatrix}}_{\dot{x}} = \underbrace{\begin{bmatrix} 0_{2 \times 2} & I_{2 \times 2} \\ 0_{2 \times 2} & 0_{2 \times 2} \end{bmatrix}}_{f(x)} \underbrace{\begin{bmatrix} p \\ v \end{bmatrix}}_{g(x)} + \underbrace{\begin{bmatrix} 0_{2 \times 2} \\ I_{2 \times 2} \end{bmatrix}}_{g(x)} u, \quad (5)$$

where $p = [p_x, p_y]^\top$, $v = [v_x, v_y]^\top$, and $u = [u_x, u_y]^\top \in \mathbb{R}^2$ denote the position, velocity, and control inputs, respectively.

Assume that there exist multiple prior unknown obstacles \mathcal{O}_l in an environment \mathcal{E} , where $l \in \mathcal{L} := \{l | l = 1, 2, \dots, L\}$ and $L \in \mathbb{N}^+$ is an uncertain value. The objective is to design a feedback controller u to drive the mobile robot (5) to safely navigate in an uncertain environment \mathcal{E} and finally reach the predetermined target position $p_d \in \mathbb{R}^2$. We formulate the safe autonomous navigation problem mentioned above as a constrained optimization problem stated as

$$\min_u J = \int_{t_0}^{t_f} u^\top u dt \quad (6a)$$

$$\text{s.t. } \dot{x} = f(x) + g(x)u \quad (6b)$$

$$p(t_0) = p_0; v(t_0) = v_0 \quad (6c)$$

$$u(t) \in \mathcal{U}, \forall t \in [t_0, t_f] \quad (6d)$$

$$p(t) \cap \bigcup_{l=1}^L \mathcal{O}_l = \emptyset, \forall t \in [t_0, t_f] \quad (6e)$$

$$\|p(t_f) - p_d\| \leq \delta, \quad p_d \in \bar{\mathcal{E}}. \quad (6f)$$

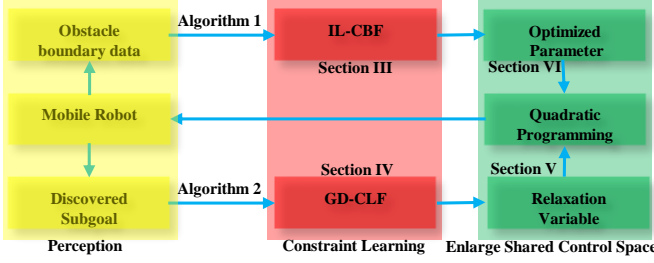


Fig. 1: Schematic of the proposed integrated perception and control approach that map raw sensory data to motion commands. The IL-CBFs learned from sensory data characterize the boundaries of obstacles as illustrated in Section III; The long-horizon task is decomposed into sequent short-horizon subtasks that are reflected by GD-CLFs introduced in Section IV; An optimization process to enlarge the shared control space is conducted in Section VI to improve the feasibility of the QP in Section V wherein IL-CBFs and GD-CLFs are incorporated.

where $\delta \in \mathbb{R}^+$ in (6f) is a prior set threshold to check whether the task is completed. $\mathcal{U} \subseteq \mathbb{R}^2$ in (6d) denotes the bounded input space of the considered dynamics (6b). A quadratic control energy function is adopted in (6a) to reflect controllers' preference on the minimization of control efforts.

The aforementioned safe autonomous navigation problem (6) is nontrivial given the constraints indicating different (might conflicting) objectives of safety and performance, and the requirement of constraint satisfaction under uncertainty (limited knowledge of the environment \mathcal{E}). This work seeks for an integrated perception and control (end-to-end) approach to solve (6), whose mechanism is illustrated in Fig.1. In particular, we directly use perceptual inputs to learn IL-CBFs and GD-CLFs that are used in the control level to achieve collision avoidance and accomplish given tasks. Note that in the following, we firstly construct IL-CBFs and GD-CLFs assuming that $\mathcal{U} = \mathbb{R}^2$ for convenience, i.e., there is no constraint on the input. This is because the construction of CBFs and CLFs within consideration of input saturation still remains an open problem [6], [33]. Then, we analyse the potential conflicts between IL-CBF, GD-CLF and input constraints.

III. IL-CBF ONLINE LEARNING

This section elucidates the mechanism of learning IL-CBFs from sensory data. In particular, the detected local obstacle information is utilized to learn a barrier function to describe the obstacle boundary. The developed IL-CBFs are employed to formulate the QP problem in Section V to conduct collision avoidance with prior-unseen obstacles in the control level.

As illustrated in Fig.2, the whole boundaries of the obstacles \mathcal{O}_l in \mathcal{E} could be described by the barrier functions $h_l(p) : \mathbb{R}^2 \rightarrow \mathbb{R}$ using the complete knowledge of obstacles [6]. However, the obstacle information is unavailable in our interested safe autonomous navigation problem (6). Thus, the explicit forms of $h_l(p)$ that characterize the dangerous region $\bigcup_{l=1}^L \mathcal{O}_l$ are unavailable. We observe in Fig.2 that partial obstacle boundaries of \mathcal{O}_l pose threats to the safety of the mobile robot at certain period. This motivates us to utilize local sensory data to learn

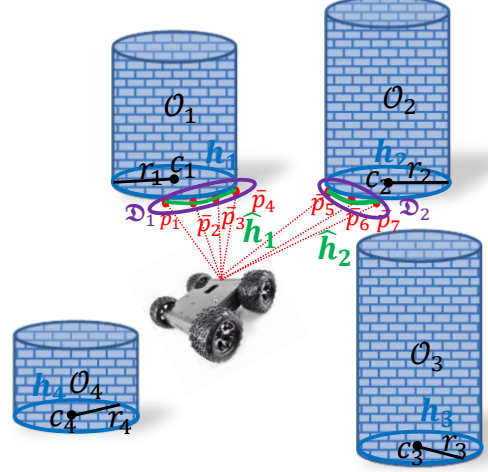


Fig. 2: Graphical illustration of IL-CBFs and obstacles. The whole boundary of obstacles \mathcal{O}_l are described by explicit CBFs $h_l = (x - x_{o_l})^2 + (y - y_{o_l})^2 - r_l^2$, $c_l = (x_{o_l}, y_{o_l})$, $l = 1, 2, 3, 4$. The mobile robot observes $\mathcal{D} = \{\bar{p}_1, \bar{p}_2, \dots, \bar{p}_7\}$ and classifies \mathcal{D} into sub-groups \mathcal{D}_k , $k = 1, 2$. Thus, $K = 2$, and $I_1 = 4$, $I_2 = 3$ here. The mobile robot learns \hat{h}_k based on \mathcal{D}_k .

the IL-CBFs corresponding to the partial obstacle boundary within the mobile robot's sensor horizon.

Assume that the mobile robot is embedded with a light detection and ranging (LiDAR) sensor with a restricted angle S_θ and a limited horizon S_r . The value of S_θ is given, and the value of S_r satisfies

$$S_r \geq D_{\text{brake}} := \|v_{\text{max}}\|^2 / \|a_{\text{max}}\|, \quad (7)$$

where $v_{\text{max}}, a_{\text{max}} \in \mathbb{R}^2$ are the maximum velocity and breaking acceleration of the mobile robot (5). D_{brake} denotes the travelled distance when the mobile robot with the maximum velocity brakes using the maximum breaking acceleration.

Remark 1. The setting of the sensor horizon (7) is beneficial to the emergence case where our developed safe feedback control strategy fails to guarantee safety. In this scenario, the mobile robot brakes to avoid collisions.

The LiDAR sensor provides a point cloud \mathcal{L} . We term $\mathcal{D} := \{\bar{p}_1, \bar{p}_2, \dots\} \subset \mathcal{L}$ as the data group of the sensed obstacle boundaries, wherein $\bar{p}_i = [\bar{x}_i, \bar{y}_i]^\top \in \mathbb{R}^2$ denotes the position of the i -th detected obstacle boundary point. In an environment \mathcal{E} with densely populated obstacles, data points in \mathcal{D} might concern multiple isolated obstacles, as displayed in Fig.2. Therefore, we adopt the robust classifying algorithm—density-based spatial clustering of applications with noise (DBSCAN) [34]—to classify \mathcal{D} into multiple sub-groups $\mathcal{D}_k = \{\bar{p}_{k_1}, \bar{p}_{k_2}, \dots\}$, wherein $\bar{p}_{k_i} = [\bar{x}_{k_i}, \bar{y}_{k_i}]^\top \in \mathbb{R}^2$ denotes the i -th detected obstacle boundary point of the k -th data group, $i \in \mathcal{I} = \{i | i = 1, \dots, I_k\}$ with $I_k \in \mathbb{N}^+$ being the volume of \mathcal{D}_k , and $k \in \mathcal{K} = \{k | k = 1, \dots, K\}$ with $K \in \mathbb{N}^+$ being the sum of the local obstacle boundary considered in current period.

Remark 2. Both the values of I_k and K are determined automatically by the DBSCAN algorithm. The explicit values of K and I_k are affected by multiple factors, e.g., the relative position between the mobile robot and obstacles, the shape of obstacles, the sensor horizon, etc. The volume of each data group \mathcal{D}_k relates with the trade-off between accuracy (separation between safe and dangerous regions) and speed (the fewer data, the smaller computation load).

In the following, we clarify the mechanism of the IL-CBF learning focusing on the k -th data group \mathcal{D}_k . Assume that i -th data pair \bar{p}_{k_i} follows

$$\bar{y}_{k_i} = \mathcal{F}(\bar{x}_{k_i}, \zeta_k) + \varepsilon_k, \quad (8)$$

where $\mathcal{F}(\bar{x}_{k_i}, \zeta_k)$ is a n degree polynomial function with a to be learned parameter $\zeta_k \in \mathbb{R}^{n+1}$, and $\varepsilon_k \sim N(0, \sigma^2)$ denotes an assumed Gaussian sensor noise with zero mean and constant variance $\sigma \in \mathbb{R}$.

Remark 3. There exist multiple choices for \mathcal{F} , such as Gaussian models, linear fitting, and rational polynomials [35]. Considering the generality and simplicity issues, a polynomial model is chosen here.

Based on (8) and the point cloud \mathcal{D}_k from the LiDAR sensor, ζ_k is learned to minimize the approximation error:

$$\hat{\zeta}_k = \arg \min_{\zeta_k} \sum_{i=1}^{I_k} (\bar{y}_{k_i} - \mathcal{F}(\bar{x}_{k_i}, \zeta_k))^2. \quad (9)$$

To counter noises and outliers that exist in the measurement data, the robust regression technique—*M-estimate* [36], [37]—is adopted here. By using the *M-estimate*, the learning of ζ_k in (9) is rewritten as

$$\hat{\zeta}_k = \arg \min_{\zeta_k} \sum_{i=1}^{I_k} \rho \left(\frac{\bar{y}_{k_i} - \mathcal{F}(\bar{x}_{k_i}, \zeta_k)}{\gamma} \right), \quad (10)$$

where $\rho(r) = c^2 / (1 - (1 - (r/c)^2)^3)$ is a robust loss function with $c = 1.345$; γ is a scale parameter estimated as $\gamma = 1.48 [\text{med}_i |(\bar{y}_{k_i} - \mathcal{F}(\bar{x}_{k_i}, \zeta_{k_0})) - \text{med}_i (\bar{y}_{k_i} - \mathcal{F}(\bar{x}_{k_i}, \zeta_{k_0}))|]$ with ζ_{k_0} being the initial value of ζ_k . More details about the *M-estimate* approach are referred to [37].

Based on the learned $\hat{\zeta}_k$ from (10), the IL-CBF \hat{h}_k is constructed as

$$\hat{h}_k(x, y) = y - \mathcal{F}(x, \hat{\zeta}_k). \quad (11)$$

The IL-CBF online learning process mentioned above is summarized as Algorithm 1. The mobile robot uses Algorithm 1 to update the learned IL-CBFs continuously based on the newly observed sensory data during the navigation process. The IL-CBF learning enjoys computation simplicity. Thus, it is practical for the mobile robot to update the learned IL-CBFs each step, which is favourable to achieve collision avoidance with dynamic obstacles and even other mobile robots ¹.

Remark 4. As the mobile robot moves forward the target position, more sensory data about obstacle boundaries are

Algorithm 1 The IL-CBF Online Learning Algorithm

Input: Point cloud \mathcal{D} ;

Output: $\hat{h}_k, k = 1, \dots, K$;

- 1: $K = \text{DBSCAN}(\mathcal{D})$ ▷ Robust classifying
 - 2: **for** $k = 1 : K$ **do**
 - 3: $\hat{\zeta}_k = \text{M-estimate}(\mathcal{D}_k)$ (10) ▷ Robust regression
 - 4: $\hat{h}_k = y - \mathcal{F}(x, \hat{\zeta}_k)$ (11)
 - 5: **end for**
-

Algorithm 2 GD-CLF Learning Algorithm

Input: Point cloud $\mathcal{A} := \{\tilde{p}_1, \tilde{p}_2, \dots\}$; Robot position p .

Output: \tilde{p}_{d_j} , and $V_j, j = 1, \dots, J$;

- 1: $\tilde{p}_{d_1} = \arg \min_{\tilde{p}_i \in \mathcal{A}} \|\tilde{p}_i - p_d\|$ and get V_1 (12)
 - 2: **if** $\|p - \tilde{p}_{d_j}\| \leq \delta$ **then**
 - 3: $\tilde{p}_{d_j} = \arg \min_{\tilde{p}_i \in \mathcal{A}} \|\tilde{p}_i - p_d\|$
 - 4: $j = j + 1$ and update V_j (12)
 - 5: **end if**
-

acquired by the LiDAR sensor. Alternatively, we are able to realize the IL-CBF learning in an incremental way along with a steady stream of data, i.e., attempting to learn one CBF that describes the whole obstacle boundary more accurate. However, authors found in practice that this increment learning approach shows no obvious advantage in terms of collision avoidance but introduces additional computation loads comparing to Algorithm 1. Thus, we forgo building a perfect map rather only using instantaneous sensory information.

Remark 5. The IL-CBF learning is especially compatible with low-end sensors that only provide low-dimensional data. These limited data, however, is not enough to build a perfect map or describe the whole obstacle boundary.

IV. GD-CLF AUTOMATIC CONSTRUCTION

This section utilizes the local collision-free sensory data group $\mathcal{A} := \mathcal{L} \ominus \mathcal{D}$ to discover sub-goals and further to construct GD-CLFs. These automatically constructed GD-CLFs serve as constraints of the QP problem in Section V, whose solution ensures that the mobile robot incrementally travel toward the discovered sub-goals and finally reach the destination.

Normally, the common CLF in Definition 2 is inefficient to account for a long-horizon goal. Thus, through a divide-and-conquer perspective, this work uses sensory data \mathcal{A} to discover the sub-goals $\tilde{p}_{d_j} = [x_{d_j}, y_{d_j}]^\top \in \mathbb{R}^2$ based on a Euclidean distance metric, $j \in \mathcal{J} = \{j | j = 1, \dots, J\}$ with $J \in \mathbb{N}^+$. These automatically determined intermediate waypoints (such as \tilde{p}_{d_1} , \tilde{p}_{d_2} , and \tilde{p}_{d_3} in Fig.3) forwardly progress toward the final desired position p_d . In particular, we choose the nearest collision-free waypoint toward the goal position p_d as the next sub-goal (line 3 of Algorithm 2).

The automatically determined sub-goals \tilde{p}_{d_j} from Algorithm 2 divide the long-horizon task into J short-horizon subtasks. To complete each subtask, we construct the GD-CLF :

$$V_j = (p - \tilde{p}_{d_j})^\top P (p - \tilde{p}_{d_j}) + (v - v_{d_j})^\top Q (v - v_{d_j}), j \in \mathcal{J} \quad (12)$$

where $P, Q \in \mathbb{R}^{2 \times 2}$ are predetermined positive definite matrices; and $v_{d_j} \in \mathbb{R}^2$ could be a zero or a constant velocity

¹A supplemental video to avoid moving obstacle is referred to <https://youtu.be/aBcj7SUmlDU>

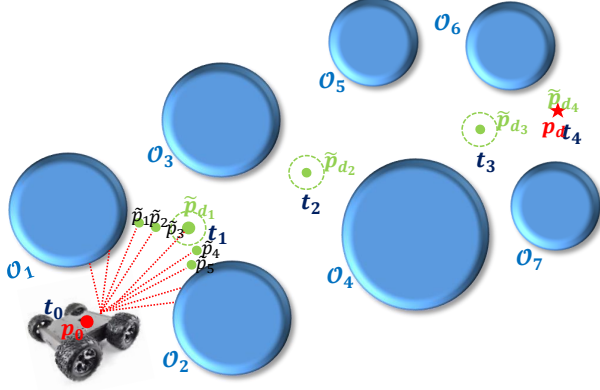


Fig. 3: Graphical illustration of GD-CLFs and subgoals. The mobile robot uses the collision-free data group $\mathfrak{A} = \{\tilde{p}_1, \tilde{p}_2, \dots, \tilde{p}_5\}$ and Algorithm 2 to determine the data point $\tilde{p}_3 \in \mathfrak{A}$ as its first subgoal \tilde{p}_{d1} . Then, the constructed GD-CLF V_1 guides the mobile robot toward \tilde{p}_{d1} . The mobile robot would determine the $j+1$ -th sub-goal when it arrives at δ -neighbourhood around the j -th sub-goal (described as a green circle with radius δ).

vector. The constructed GD-CLF V_j (12) updates as the subgoal \tilde{p}_{dj} refreshes.

V. SAFE FEEDBACK CONTROL STRATEGY

This section utilizes the learned IL-CBFs in Section III and the constructed GD-CLFs in Section IV to generate the safe feedback control strategy that drives the mobile robot to safely navigate to the target position incrementally.

By dividing the period $[t_0, t_f]$ into multiple intervals $[t_0 + mT, t_0 + (m+1)T]$ [28], where $m \in \mathbb{N}^+$, and $T \in \mathbb{R}^+$ is the sampling time, and within consideration of the learned IL-CBFs (11) and the constructed GD-CLFs (12), we reformulate the original safe autonomous navigation problem (6) into a sequence of QPs at each interval:

$$\min_{u, \nu} u(t)^\top u(t) + c_1 \nu^2(t) \quad (13a)$$

$$\text{s. t. (6b), (6c), (6d)}$$

$$\ddot{h}_k + \alpha_{k1} \dot{h}_k + \alpha_{k2} h_k \geq 0, \quad k \in \mathcal{K} \quad (13b)$$

$$\dot{V}_j + c_2 V_j \leq \nu, \quad j \in \mathcal{J}, \quad (13c)$$

where $\nu(t) \in \mathbb{R}$ is a relaxation variable to relax the GD-CLF constraint [38]; $c_1 \in \mathbb{R}$ is a penalty on the relaxation variable $\nu(t)$; α_{k1}, α_{k2} and $c_2 \in \mathbb{R}$ are parameters to be determined. The reformulated QP problem (13) unifies safety (6d), (13b), task requirements (13c), and optimization over control efforts (13a) to generate a multi-objective controller that drives the mobile robot to progressively reach subgoals while avoid obstacles. Note that the safe feedback control strategy from (13) only requires the position information of the mobile robot p and the target p_d .

VI. OPTIMIZED ADMISSIBLE CONTROL SPACE

This section attempts to solve the potential conflicts between constraints (6d), (13b), and (13c) of the QP problem formulated in Section V.

For analytical convenience, we denote the admissible control spaces (ACSs) for constraints (13b) and (13c) as $\mathcal{A}_1 = \{u \in \mathbb{R}^2 | \ddot{h}_k + \alpha_{k1} \dot{h}_k + \alpha_{k2} h_k \geq 0, k \in \mathcal{K}\}$, and $\mathcal{A}_2 = \{u \in \mathbb{R}^2 | \dot{V}_j + c_2 V_j \leq \nu\}$, respectively. Thereby, the shared control space concerning constraints (6d), (13b), and (13c) is termed as $\mathcal{S} = \mathcal{A}_1 \cap \mathcal{A}_2 \cap \mathcal{U}$. It is desirable that $\mathcal{S} \neq \emptyset$ always holds, i.e., the feasibility of the QP problem is always guaranteed. This is a nontrivial problem, especially multiple constraints are considered. Improving the possibility of satisfying $\mathcal{S} \neq \emptyset$ is equivalent to enlarge the volume of \mathcal{S} . Given that the relationship between sets \mathcal{A}_1 and \mathcal{A}_2 is hard to be described and the volume of \mathcal{U} is predetermined, we are able to transform the enlargement of the volume \mathcal{S} into the enlargement of the volumes of ACSs \mathcal{A}_1 and \mathcal{A}_2 independently. A relaxation variable ν has been used in (13c) to enlarge the volume of \mathcal{A}_2 . In the following, we attempt to enlarge the volume of the ACS \mathcal{A}_1 to improve the feasibility of the QP problem (13). In particular, we firstly seek for a criterion for the volume of the ACS \mathcal{A}_1 in Section VI-A by investigating the relationship between sets \mathcal{A}_1 and \mathcal{U} . Then, a linear programming (LP) optimization problem is formulated in Section VI-B to enlarge the volume of the ACS \mathcal{A}_1 .

A. Criterion of ACS

The enlargement of \mathcal{A}_1 is equivalent to enlarge each IL-CBF \hat{h}_k associated ACS denoted as \mathcal{A}_{1k} , $k \in \mathcal{K}$. The explicit form of the learned k -th IL-CBF follows $\hat{h}_k = y - \hat{\zeta}_k^\top \Phi$, where $\Phi = [1, x, x^2, \dots]$. To get an intuitive illustration of \mathcal{A}_{1k} , we substitute \hat{h}_k into (13b) and rewrite the inequality focusing on control inputs:

$$A u_x + u_y + a_k^\top \Psi > 0, \quad (14)$$

where $A = \hat{\zeta}_k^\top \partial \Phi x \in \mathbb{R}$, $\alpha_k = [\alpha_{k1}, \alpha_{k2}]^\top \in \mathbb{R}^2$, $\Psi = [\hat{\zeta}_k^\top \partial \Phi x v_x - v_y, \hat{\zeta}_k^\top \partial [2] \Phi x v_x^2 + \hat{\zeta}_k^\top \Psi - y]^\top \in \mathbb{R}^2$.

Based on the reformulated (14), the geometric interpretations of the ACS \mathcal{A}_{1k} as well as the limited control input set \mathcal{U} are depicted in Fig.4. We found that a large value of $a_k^\top \Psi$ leads to a larger area of the ACS \mathcal{A}_{1k} . Thus, it is reasonable to choose the value of $a_k^\top \Psi$ as a metric to quantify the volume of the ACS \mathcal{A}_{1k} , which is optimized in the subsequent subsection.

B. Optimization of ACS

This subsection clarifies the optimization over the metric $a_k^\top \Psi$, which is formulated as a LP problem:

$$\min_{\alpha_k} \alpha_k^\top \Psi \quad (15a)$$

$$\text{s. t. } 0 < \alpha_{k1}, \alpha_{k2} < \bar{\alpha}_k \quad (15b)$$

$$a_{k1}^2 - 4\alpha_{k2} \geq 0 \quad (15c)$$

where $\bar{\alpha}_k \in \mathbb{R}^+$ is the predetermined bound for the optimization variable. The core idea is to select suitable values of α_{k1} and

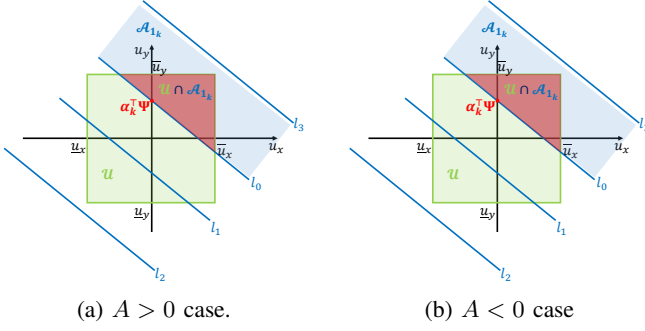


Fig. 4: The geometric interpretation of the sets \mathcal{A}_{1_k} and \mathcal{U} . Here $l_k = Au_x + u_y + a_k^\top \Psi = 0$. The comparison of the volume of \mathcal{A}_{1_k} follows $\mathcal{A}_{1_k}^{l_2} > \mathcal{A}_{1_k}^{l_1} > \mathcal{A}_{1_k}^{l_0} > \mathcal{A}_{1_k}^{l_3}$ for two cases. For the l_3 case, $\mathcal{A}_{1_k} \cap \mathcal{U} = \emptyset$, i.e., there is no feasible control input to ensure safety based on current chosen IL-CBF.

α_{k2} to enlarge the volume of \mathcal{A}_{1_k} . The formulated LP problem (15) is solved by the off-the-self *fmincon* solver.

Remark 6. The constraints (15b) and (15c) are a simplification of the following three constraints: (1) $a_{k1}^2 - 4\alpha_{k2} \geq 0$; (2) $-\alpha_{k1} + \sqrt{a_{k1}^2 - 4\alpha_{k2}} < 0$; (3) $\frac{-\alpha_{k1} - \sqrt{a_{k1}^2 - 4\alpha_{k2}}}{2} < 0$. These three constraints ensure that the roots of (13b)'s related polynomials are all negative. These constraints ensure that the optimized parameter α_k^* leads to valid HO-CBFs in Definition 1.

VII. NUMERICAL SIMULATIONS

This section conducts numerical simulations to validate the efficiency of our proposed safe feedback control strategy. In particular, Section VII-A presents the benefits brought by the enlargement of the ACS \mathcal{A}_1 . Then, we validate the efficiency of the safe feedback control strategy under an obstacle-filled outdoor navigation scenario in Section VII-B, and a maze indoor navigation scenario in Section VII-C.

A. Validation of optimized ACS

This subsection validates the effectiveness of our developed optimized ACS strategy (15) clarified in Section VI-B based on a benchmark reach-avoid task. A mobile robot modelled as (5) is desired to move from an initial position p_0 to a desired position p_d while avoiding one circle obstacle \mathcal{O} (centered at $c = (1, 1)$ and with radius $r = 1$) during the navigation process. The detailed simulation settings are referred to Table I. Note that to avoid IL-CBFs and GD-CLFs' influence to the solution feasibility, this subsection uses a prior-known CBF to achieve collision avoidance, and a Proportional-Derivative (PD) controller is assumed to accomplish the reach task with desired performance.

TABLE I: The parameter settings of the reach-avoid task.

Initial values	$p_0 = [-0.2, 0.1]^\top$, $v_0 = [0, 0]^\top$, $T = 10\text{Hz}$
Target values	$p_d = [2, 1.5]^\top$, $v_d = [0, 0]^\top$
CBF	$h = (x-1)^2 + (y-1)^2 - 1$
PD controller	$u_{pd} = -0.2(p - p_d) - 0.9(v - v_d)$
QP and LP	$\bar{u}_x/\bar{u}_y = 0.3$, $\alpha_1(t_0) = [5, 6]^\top$, $\bar{\alpha}_1 = 7$.

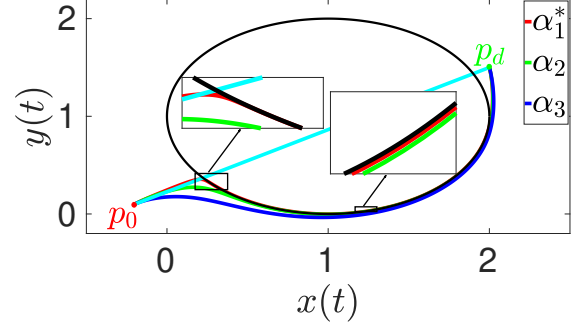


Fig. 5: The comparison regarding trajectories.

We formulate the following QP optimization problem (16) to solve the reach-avoid problem mentioned above.

$$\min_u \|u - u_{pd}\|^2 \quad (16a)$$

$$\text{s. t. } -0.3 < u_x, u_y < 0.3 \quad (16b)$$

$$\ddot{h} + \alpha_{11}^* \dot{h}_k + \alpha_{12}^* \hat{h} \geq 0, \quad (16c)$$

where α_{11}^* and α_{12}^* are the optimized variables after solving the LP problem (15) based on the known CBF h . For comparison, prior-chosen constant vectors $\alpha_2 = [4, 1]^\top$, $\alpha_3 = [4, 2]^\top$ are picked to construct the constraint (16c).

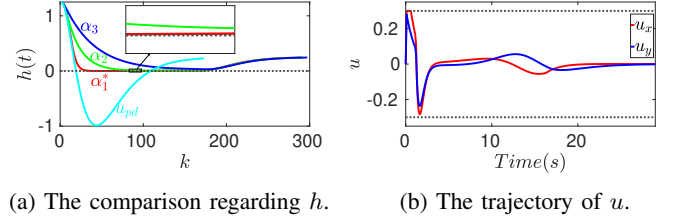


Fig. 6: The performance comparison between the optimized α_1^* and the predetermined α_2 , α_3 associated QP solutions.

As displayed in Fig.5, the mobile robot driven by the nominal u_{pd} collides with the obstacle \mathcal{O} , while a CBF based QP optimization minimally revise u_{pd} to generate a safe control input. Furthermore, as shown in Fig.5, the trajectory of the optimized α^* case navigates tighter around the obstacle as consequence of enlarged ACS, i.e., closer to the desired trajectory associated with u_{pd} . The evolution trajectory of $h(t)$ displayed in Fig.6a further validates the conclusion mentioned above. The input constraint holds as presented in Fig.6b.

B. Validation in an outdoor navigation scenario

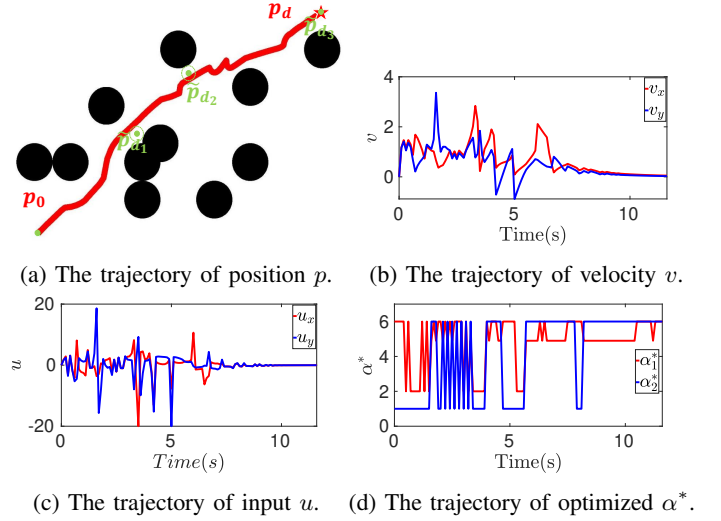
This subsection validates the efficiency of our proposed safe feedback control strategy (13) in an obstacle densely cluttered environment. The numerical simulation is conducted on the basis of the Mobile Robotics Simulation Toolbox [39] and the quadprog solver of the Optimization Toolbox [40]. The detailed parameter settings to solve the formulated QP (13) and LP (15) are presented in Table II.

It is shown in Fig.7a-7d that the mobile robot exploits sensed obstacle boundary data to identify IL-CBFs \hat{h}_1 , \hat{h}_2 based on

TABLE II: The parameter settings of outdoor navigation.

Initial values	$p_0 = [2, 4]^T, v_0 = [1, 1]^T, T = 10\text{Hz}$
Target values	$p_d = [10, 10]^T, v_d = [0, 0]^T$
IL-CBF	$\Phi = [1, x, x^2], S_\theta = [-\pi/2, \pi/2], S_r = 0.5m$
GD-CLF	$P = \begin{bmatrix} 25 & 12.5 \\ 12.5 & 25 \end{bmatrix}, Q = \begin{bmatrix} 50 & 25 \\ 25 & 50 \end{bmatrix},$ $S_\theta = [-\pi, \pi], S_r = 4m, \bar{c}_2 = 1.5$
QP and LP	$\bar{u}_x/\bar{u}_y = 20, c_1 = 1, \alpha(t_0) = [5, 6]^T, \bar{\alpha} = 6$

Algorithm 1, and uses collision-free data to discover sub-goals $\tilde{p}_{d_1}, \tilde{p}_{d_2}$ via Algorithm 2. As displayed in Fig.8a, the mobile robot safely travels toward subgoals $\tilde{p}_{d_1}, \tilde{p}_{d_2}$ sequentially and finally reach the destination p_d (same with \tilde{p}_{d_3}). For completeness, the evolution trajectories of velocity, control inputs, and the optimized parameter α^* are displayed in Fig.8b, Fig.8c, and Fig.8d, respectively. A supplemental video for the outdoor navigation scenario is referred to <https://youtu.be/mY4wPeRd3iQ> and <https://youtu.be/LXC7UOfUc5A>.

Fig. 8: The trajectories of position p , velocity v , control input u , and optimized α^* for the outdoor navigation scenario.

<https://youtu.be/4Lv6KEaYVIM> and <https://youtu.be/vegQRAhrFEk>.

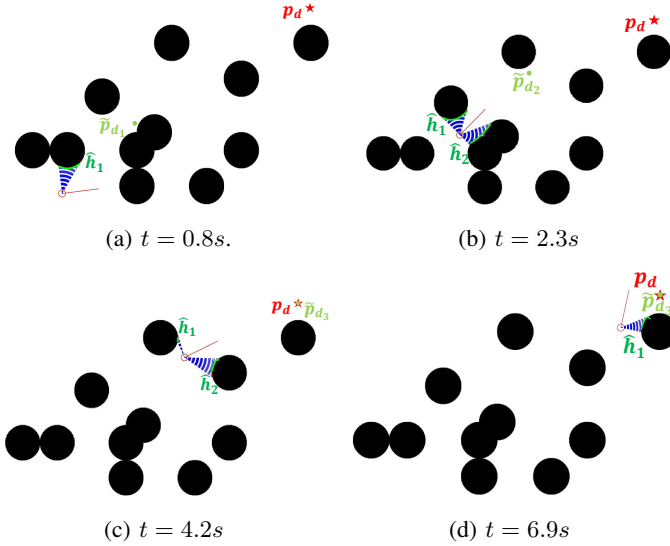


Fig. 7: The illustration of the outdoor navigation case at different time indexes.

C. Validation in an indoor navigation scenario

This subsection further validates the effectiveness of our designed safe feedback control strategy in a maze simulation environment. It is worth mentioning that the application of CBFs in a maze environment is seldom found in existing works given that multiple common CBFs are required to achieve collision avoidance in a maze environment, and certain CBFs would unavoidably treat collision-free space as unsafe region. In particular, for the maze environment displayed in Fig.9, it is nontrivial to design barrier functions to separate safe and unsafe regions even though we have the full knowledge of the environment. However, our developed IL-CBFs can efficiently deal with this indoor navigation scenario. The detailed parameters to realize the safe autonomous navigation in the maze environment is displayed in Table III. Accompanying simulation videos are available at <https://youtu.be/1OcOLPRIC6I>, <https://youtu.be/4Lv6KEaYVIM> and <https://youtu.be/vegQRAhrFEk>.

TABLE III: The parameter settings of indoor navigation.

Initial values	$p_0 = [2, 2]^T, v_0 = [0, 0]^T, T = 10\text{Hz}$
Target values	$p_d = [22, 18]^T, v_d = [0, 0]^T$
IL-CBF	$\Phi = [1, x, x^2], S_\theta = [-\pi/2, \pi/2], S_r = 0.5m$
GD-CLF	$P = \begin{bmatrix} 25 & 12.5 \\ 12.5 & 25 \end{bmatrix}, Q = \begin{bmatrix} 50 & 25 \\ 25 & 50 \end{bmatrix},$ $S_\theta = [-\pi, \pi], S_r = 4m, \bar{c}_2 = 1.5$
QP and LP	$\bar{u}_x/\bar{u}_y = 20, c_1 = 1, \alpha(t_0) = [5, 6]^T, \bar{\alpha} = 6$

As displayed in Fig.9 and Fig.10a, the mobile robot navigates safely in the maze environment and finally reach the goal position p_d . However, we acknowledge that the simple heuristic (i.e., shortest distance rule) used in Algorithm 2 leads to inefficient navigation, as shown in the blue rectangle of Fig.10a. The trajectories of the mobile robot's velocity, control input and optimized α^* are displayed in Fig.10b, Fig.10c, and Fig.10d, respectively.

VIII. CONCLUSION AND DISCUSSION

This work presents an end-to-end policy that couples sensor with control to achieve safe autonomous navigation in uncertain environments. Our developed IL-CBFs are united with GD-CLFs in a constrained optimization framework to generate safe feedback control strategies. Our method is in essence a local and reactive method. Thus, comparing to the global method, the solution might trap in local minimum. The future work aims to extend this work to a high-dimensional system and also analyze the influence of model uncertainties and environmental disturbances to the safe feedback control strategy.

REFERENCES

- [1] N. Hudson, F. Talbot, M. Cox, J. Williams, T. Hines, A. Pitt, B. Wood, D. Froustheger, K. L. Surdo, T. Molnar *et al.*, "Heterogeneous ground and air platforms, homogeneous sensing: Team csiro data61's approach to the darpa subterranean challenge," *arXiv preprint arXiv:2104.09053*, 2021.

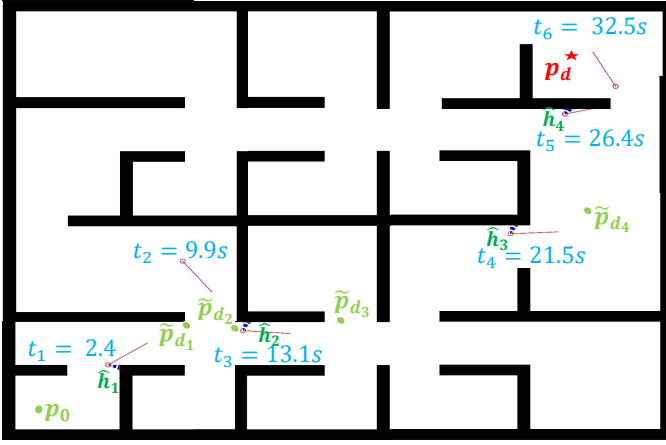


Fig. 9: The illustration of the indoor navigation case at different time indexes.

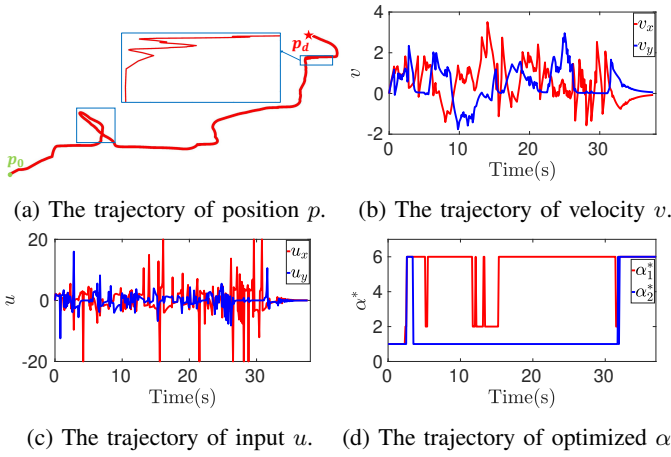


Fig. 10: The trajectories of position p , velocity v , control input u , and optimized α^* for the indoor navigation scenario.

[2] J. Higgins and N. Bezzo, "Negotiating visibility for safe autonomous navigation in occluding and uncertain environments," *IEEE Robotics and Automation Letters*, vol. 6, no. 3, pp. 4409–4416, 2021.

[3] S. M. LaValle, *Planning algorithms*. Cambridge university press, 2006.

[4] D. González, J. Pérez, V. Milanés, and F. Nashashibi, "A review of motion planning techniques for automated vehicles," *IEEE Transactions on Intelligent Transportation Systems*, vol. 17, no. 4, pp. 1135–1145, 2015.

[5] F. Gao, L. Wang, B. Zhou, X. Zhou, J. Pan, and S. Shen, "Teach-repeat-replan: A complete and robust system for aggressive flight in complex environments," *IEEE Transactions on Robotics*, vol. 36, no. 5, pp. 1526–1545, 2020.

[6] A. D. Ames, X. Xu, J. W. Grizzle, and P. Tabuada, "Control barrier function based quadratic programs for safety critical systems," *IEEE Transactions on Automatic Control*, vol. 62, no. 8, pp. 3861–3876, 2016.

[7] M. Jankovic, "Robust control barrier functions for constrained stabilization of nonlinear systems," *Automatica*, vol. 96, pp. 359–367, 2018.

[8] V. Sunkara, A. Chakravarthy, and D. Ghose, "Collision avoidance of arbitrarily shaped deforming objects using collision cones," *IEEE Robotics and Automation Letters*, vol. 4, no. 2, pp. 2156–2163, 2019.

[9] E. Rimón and D. E. Koditschek, "Exact robot navigation using artificial potential functions," *Departmental Papers (ESE)*, p. 323, 1992.

[10] H. G. Tanner and A. Boddu, "Multiagent navigation functions revisited," *IEEE Transactions on Robotics*, vol. 28, no. 6, pp. 1346–1359, 2012.

[11] B. Ichter, J. Harrison, and M. Pavone, "Learning sampling distributions for robot motion planning," in *2018 IEEE International Conference on Robotics and Automation (ICRA)*. IEEE, 2018, pp. 7087–7094.

[12] I. M. Mitchell, A. M. Bayen, and C. J. Tomlin, "A time-dependent

hamilton-jacobi formulation of reachable sets for continuous dynamic games," *IEEE Transactions on automatic control*, vol. 50, no. 7, pp. 947–957, 2005.

[13] F. S. Barbosa, L. Lindemann, D. V. Dimarogonas, and J. Tumova, "Provably safe control of lagrangian systems in obstacle-scattered environments," *arXiv preprint arXiv:2009.02148*, 2020.

[14] S. Yaghoubi, G. Fainekos, and S. Sankaranarayanan, "Training neural network controllers using control barrier functions in the presence of disturbances," *arXiv preprint arXiv:2001.08088*, 2020.

[15] H. Zhao, X. Zeng, T. Chen, and Z. Liu, "Synthesizing barrier certificates using neural networks," in *Proceedings of the 23rd International Conference on Hybrid Systems: Computation and Control*, 2020, pp. 1–11.

[16] W. Jin, Z. Wang, Z. Yang, and S. Mou, "Neural certificates for safe control policies," *arXiv preprint arXiv:2006.08465*, 2020.

[17] P. Jagtap, G. J. Pappas, and M. Zamani, "Control barrier functions for unknown nonlinear systems using gaussian processes," in *2020 59th IEEE Conference on Decision and Control (CDC)*. IEEE, 2020, pp. 3699–3704.

[18] M. Saveriano and D. Lee, "Learning barrier functions for constrained motion planning with dynamical systems," in *IEEE/RSJ International Conference on Intelligent Robots and Systems (IROS 2018) I*, 2019.

[19] A. Robey, H. Hu, L. Lindemann, H. Zhang, D. V. Dimarogonas, S. Tu, and N. Matni, "Learning control barrier functions from expert demonstrations," *arXiv preprint arXiv:2004.03315*, 2020.

[20] M. Srinivasan, A. Dabholkar, S. Coogan, and P. Vela, "Synthesis of control barrier functions using a supervised machine learning approach," *arXiv preprint arXiv:2003.04950*, 2020.

[21] R. A. Freeman and J. A. Primbs, "Control lyapunov functions: New ideas from an old source," in *Proceedings of 35th IEEE Conference on Decision and Control*, vol. 4. IEEE, 1996, pp. 3926–3931.

[22] R. A. Freeman, *Robust control of nonlinear systems*. University of California, Santa Barbara, 1995.

[23] Y.-C. Chang, N. Roohi, and S. Gao, "Neural lyapunov control," *arXiv preprint arXiv:2005.00611*, 2020.

[24] A. Abate, D. Ahmed, M. Giacobbe, and A. Peruffo, "Formal synthesis of lyapunov neural networks," *IEEE Control Systems Letters*, vol. 5, no. 3, pp. 773–778, 2020.

[25] L. Wang, A. D. Ames, and M. Egerstedt, "Safety barrier certificates for collisions-free multirobot systems," *IEEE Transactions on Robotics*, vol. 33, no. 3, pp. 661–674, 2017.

[26] G. Notomista and M. Egerstedt, "Persistence of robotic tasks," *IEEE Transactions on Control Systems Technology*, vol. 29, no. 2, pp. 756–767, 2020.

[27] B. Capelli, C. Secchi, and L. Sabattini, "Passivity and control barrier functions: Optimizing the use of energy," *IEEE Robotics and Automation Letters*, 2022.

[28] W. Xiao and C. Belta, "High order control barrier functions," *IEEE Transactions on Automatic Control*, 2021.

[29] X. Xu, "Constrained control of input–output linearizable systems using control sharing barrier functions," *Automatica*, vol. 87, pp. 195–201, 2018.

[30] A. Balestrino, A. Caiti, and S. Grammatico, "A new class of lyapunov functions for the constrained stabilization of linear systems," *Automatica*, vol. 48, no. 11, pp. 2951–2955, 2012.

[31] S. Grammatico, F. Blanchini, and A. Caiti, "Control-sharing and merging control lyapunov functions," *IEEE Transactions on Automatic Control*, vol. 59, no. 1, pp. 107–119, 2013.

[32] A. D. Ames, K. Galloway, K. Sreenath, and J. W. Grizzle, "Rapidly exponentially stabilizing control lyapunov functions and hybrid zero dynamics," *IEEE Transactions on Automatic Control*, vol. 59, no. 4, pp. 876–891, 2014.

[33] P. Jagtap, S. Soudjani, and M. Zamani, "Formal synthesis of stochastic systems via control barrier certificates," *IEEE Transactions on Automatic Control*, 2020.

[34] M. Ester, H.-P. Kriegel, J. Sander, X. Xu *et al.*, "A density-based algorithm for discovering clusters in large spatial databases with noise." in *Kdd*, vol. 96, no. 34, 1996, pp. 226–231.

[35] J. O. Rawlings, S. G. Pantula, and D. A. Dickey, *Applied regression analysis: a research tool*. Springer Science & Business Media, 2001.

[36] Mathworks, "Curve fitting toolbox: user's guide (r2020a)," 2020.

[37] P. W. Holland and R. E. Welsch, "Robust regression using iteratively reweighted least-squares," *Communications in Statistics-theory and Methods*, vol. 6, no. 9, pp. 813–827, 1977.

[38] W. Xiao, G. C. Cassandras, and C. Belta, "Safety-critical optimal control for autonomous systems," *Journal of Systems Science and Complexity*, vol. 34, no. 5, pp. 1723–1742, 2021.

- [39] S. Castro, *Mobile Robotics Simulation Toolbox*, MathWorks, 2019. [Online]. Available: <https://github.com/mathworks-robotics/mobile-robotics-simulation-toolbox>
- [40] T. Coleman, M. A. Branch, and A. Grace, "Optimization toolbox," *For Use with MATLAB. User's Guide for MATLAB 5, Version 2, Release II*, 1999.